




# Optimal Softening for Gravitational Force Calculations in $N$ -body Dynamics

Hirakjyoti Das<sup>1,2</sup>, Sukanta Deb<sup>1,3</sup>, and Amiya Baruah<sup>2</sup> 

<sup>1</sup> Department of Physics, Cotton University, Guwahati 781001, Assam, India; [sukanta.deb@cottonuniversity.ac.in](mailto:sukanta.deb@cottonuniversity.ac.in)

<sup>2</sup> Experimental Geodynamics Laboratory, Cotton University, Guwahati 781001, Assam, India

<sup>3</sup> Space and Astronomy Research Centre (SARC), Cotton University, Guwahati 781001, Assam, India

Received 2020 November 27; revised 2021 February 4; accepted 2021 February 21; published 2021 April 19

## Abstract

The choice of the optimal value of the softening length ( $\epsilon_i$ ) of each particle dealing with  $N$ -body simulations has a profound impact on error values in the gravitational force calculation. A slight deviation from its exact optimal value may result in a large error in the calculation. In this paper we augment the accuracy of the existing gravitational force calculation methods by providing a new technique to calculate the individual optimal values of  $\epsilon_i$  for various configurations of the Plummer density model. We have proposed an expression  $\epsilon_{\lambda,i} = \lambda_i \left( \frac{m_i}{\rho_i} \right)^{\frac{1}{3}}$  that relates each particle by considering the average characteristic length ( $\lambda_i$ ) and density ( $\rho_i$ ), unlike previous studies that considered  $\epsilon_i$  as an exclusive function of  $\rho_i$ . We have performed gravitational force calculations for each and every particle from the Plummer density model using compact as well as noncompact gravitational force methods based on smoothed particle hydrodynamics. We have tested our new equation for the entire range of numerical simulations performed during the study. It is found that the errors in our force calculations are not only lower than those estimated from previous studies but also remain flat for various considerations of nearest neighboring particles ( $N_{\text{neigh}}$ ). The adjusted expression of  $\epsilon_{\lambda,i}$  in our study has less dependence on  $N_{\text{neigh}}$  in the Plummer sphere. Finally, based on the results obtained using the method proposed in this study, we find that it remarkably improves both the accuracy as well as the stability of the gravitational force calculation.

*Unified Astronomy Thesaurus concepts:* [Newtonian gravitation \(1110\)](#); [Hydrodynamical simulations \(767\)](#); [Astrophysical fluid dynamics \(101\)](#); [N-body problem \(1082\)](#)

## 1. Introduction

The gravitational  $N$ -body simulation method is one of the most widely used techniques to find a numerical solution dealing with the dynamics of  $N$  number of particles in a gravitational field (Gingold & Monaghan 1977; Rasio & Livio 1996; Bate & Burkert 1997; Asphaug et al. 2006; Price et al. 2018). In astrophysics, starting from a two-body problem like the Earth–Moon system to the large-scale structure phenomena of the universe, this technique has been quite successful in creating a better understanding of  $N$ -body dynamics. Various methods were developed to improve the speed (Barnes & Hut 1986; Katz et al. 1996; Davé et al. 1997; Lia & Carraro 2000; Schäfer et al. 2016) and accuracy (Couchman et al. 1995; Owen et al. 1998; Athanassoula et al. 2000; Dehnen 2001; Quinlan et al. 2006; Price & Monaghan 2007; Hosono et al. 2013) of the  $N$ -body simulation technique.

Among various  $N$ -body simulation methods, smoothed particle hydrodynamics (SPH) has emerged as the most successful one in dealing with gravitational  $N$ -body problems. SPH is a meshless method first introduced by Lucy (1977) to solve astrophysical problems and subsequently developed by Gingold & Monaghan (1977). It has been particularly successful in dealing with the asymmetric nature of astrophysical problems due to its remarkable adaptability and simplicity in handling large and complex systems. This method is now widely used not only to solve astrophysical problems but also in other fields like geophysics, engineering applications, and the development of computer games, etc. (Petschek & Libersky 1993; Flebbe et al. 1994; Balsara 1995; Wadsley et al. 2004; Tartakovsky & Meakin 2005; Price 2008; Federrath et al. 2010; Merlin et al. 2010; Valcke et al. 2010; Romeo Velonà et al. 2013;

Hosono et al. 2016; Bui & Nguyen 2017; Davis et al. 2019; Malamud & Perets 2020; Sun et al. 2021).

In a gravitational field consisting of  $N$  particles, the gravitational force  $F_i$  acting on an  $i$ th particle is given by

$$\mathbf{F}_i = - \sum_{j=1}^N \frac{G m_i m_j}{|\mathbf{r}_{ij}|^2} \frac{\mathbf{r}_{ij}}{|\mathbf{r}_{ij}|}, \quad (1)$$

where  $G$  is the universal constant of gravitation and  $\mathbf{r}_{ij} = \mathbf{r}_i - \mathbf{r}_j$  is the distance between the  $i$ th and the  $j$ th particle. It can be seen that the gravitational force  $\mathbf{F}_i$ , calculated using Equation (1), leads to an infinite value as the distance between the two particles approaches zero. To deal with this effect of singularity, an additional length  $\epsilon$  is added in the denominator of Equation (1). The length  $\epsilon$  is optimized so that any departure from the actual gravitational force is minimal. With the addition of the term  $\epsilon$ , the expression of  $\mathbf{F}_i^{\text{nc}}$  (noncompact force) can be obtained as

$$\mathbf{F}_i^{\text{nc}} = - \sum_{j=1}^N \frac{G m_i m_j}{(r_{ij}^2 + \epsilon^2)} \frac{\mathbf{r}_{ij}}{|\mathbf{r}_{ij}|}. \quad (2)$$

This additional length  $\epsilon$  is called the softening length and it determines the degree of smoothing. The choice of a too small value of  $\epsilon$  will result in a very noisy outcome, i.e., this leads to an unstable solution because of the very strong divergent force when the particles are very close to each other. On the other hand, too large a value of  $\epsilon$  will also lead to a biased estimate from the correct Newtonian force results (Merritt 1996; Athanassoula et al. 2000; Dehnen 2001; Rodionov & Sotnikova 2005). While keeping this fact in view, methods

were developed to determine the optimal value of  $\epsilon$ , which yields less error in the calculations. Some studies keep  $\epsilon$  fixed (Merritt 1996; Athanassoula 1998) while some others relate it to the adaptive SPH smoothing length (Price & Monaghan 2007) for the calculations.

The present study is primarily focused on finding an optimal value of  $\epsilon$  using a newly formulated adaptive method, while calculating the gravitational force with an enhanced accuracy and robustness of the results, for compact as well as noncompact forces. In Section 2 we discuss the theory and methods used in our present study. Section 3 deals with the results and analysis. Finally, the summary and conclusions of this study are presented in Section 4.

## 2. Theory and Methods

### 2.1. Lagrangian Formulation

The Lagrangian for self-gravitating particles is given by

$$L = \sum_{i=1}^N m_i \left( \frac{1}{2} v_i^2 - \phi_i - u_i \right), \quad (3)$$

where  $v_i$  denotes the velocity,  $\phi_i$  is the gravitational potential,  $u_i$  is the thermal energy, and  $m_i$  is the mass of the  $i$ th particle.

Dyer & Ip (1993) and Dehnen (2001) demonstrated that the use of the kernel smoothing approach in a compact force can significantly minimize the error in the force calculations. Later, Price & Monaghan (2007) introduced an adaptive method for a spline gravitational smoothing kernel that takes into account the respective smoothing length ( $h_i$ ) for every individual particle. Importantly, in such a kernel smoothing approach, the smoothing length ( $h_i$ ) represents the optimal value of  $\epsilon_i$ . The gravitational potential based on the cubic spline kernel is given by (Price & Monaghan 2007)

$$\phi = \begin{pmatrix} \frac{1}{h} \left[ \frac{2}{3} q^2 - \frac{3}{10} q^4 + \frac{1}{10} q^5 - \frac{7}{5} \right], & 0 \leq q < 1 \\ \frac{1}{h} \left[ \frac{4}{3} q^2 - q^3 + \frac{3}{10} q^4 - \frac{1}{30} q^5 - \frac{8}{5} + \frac{1}{15q} \right], & 1 \leq q < 2 \\ -\frac{1}{r_{ij}}, & q \geq 2. \end{pmatrix}, \quad (4)$$

where

$$q = \frac{|r_{ij}|}{h_i}.$$

The derivative of the above equation can be expressed as

$$\phi' = \begin{pmatrix} \frac{1}{h^2} \left[ \frac{4}{3} q - \frac{6}{5} q^3 + \frac{1}{2} q^4 \right], & 0 \leq q < 1 \\ \frac{1}{h^2} \left[ \frac{8}{3} q - 3q^2 + \frac{6}{5} q^3 - \frac{1}{6} q^4 - \frac{1}{15q^2} \right], & 1 \leq q < 2 \\ -\frac{1}{r_{ij}^2}, & q \geq 2. \end{pmatrix}. \quad (5)$$

For the fixed gravitational softening length, the Lagrangian consideration yields the gravitational force (compact) acting on each particle from the Euler-Lagrange equations as

(Price & Monaghan 2007)

$$\mathbf{F}_i^c = -Gm_i \sum_{j=1}^N m_j \left[ \frac{\phi'_i(h_i) + \phi'_j(h_j)}{2} \right] \frac{\mathbf{r}_{ij}}{|\mathbf{r}_{ij}|}. \quad (6)$$

Equation (6) is a symmetric form of Equation (2) obtained using

$$\phi'_i(\epsilon_i) = \frac{1}{\epsilon_i^2 + r_{ij}^2}. \quad (7)$$

On the other hand, invoking an adaptive softening length approach, the gravitational acceleration is given by

$$\frac{d\mathbf{v}_i}{dt} = -G \sum_{j=1}^N m_j \left[ \frac{\phi'_i(h_i) + \phi'_j(h_j)}{2} \right] \frac{\mathbf{r}_{ij}}{|\mathbf{r}_{ij}|} - \frac{G}{2} \sum_{j=1}^N m_j \left[ \frac{\zeta_i}{\Omega_i} \frac{\partial W_{ij}(h_i)}{\partial r_i} + \frac{\zeta_j}{\Omega_j} \frac{\partial W_{ij}(h_j)}{\partial r_i} \right], \quad (8)$$

where

$$W(r, h) = \frac{1}{\pi h^3} \begin{pmatrix} 1 - \frac{3}{2} q^2 - \frac{3}{4} q^3, & 0 \leq q < 1 \\ \frac{1}{4} (2 - q)^3, & 1 \leq q < 2 \\ 0, & q \geq 2, \end{pmatrix}, \quad (9)$$

where

$$q = \frac{|\mathbf{r}_{ij}|}{h_i}.$$

Thus the gravitational force acting on an  $i$ th particle can be expressed as (Price & Monaghan 2007)

$$\mathbf{F}_i^c = -Gm_i \sum_{j=1}^N m_j \left[ \frac{\phi'_i(h_i) + \phi'_j(h_j)}{2} \right] \frac{\mathbf{r}_{ij}}{|\mathbf{r}_{ij}|} - m_i \frac{G}{2} \sum_{j=1}^N m_j \left[ \frac{\zeta_i}{\Omega_i} \frac{\partial W_{ij}(h_i)}{\partial r_i} + \frac{\zeta_j}{\Omega_j} \frac{\partial W_{ij}(h_j)}{\partial r_i} \right], \quad (10)$$

where  $\Omega_i$  and  $\zeta_i$  are respectively given by

$$\Omega_i = \left[ 1 - \frac{\partial h_i}{\partial \rho_i} \sum_{j=1}^N m_j \frac{\partial W_{ij}}{\partial h_i} \right] \quad (11)$$

and

$$\zeta_i = \frac{\partial h_i}{\partial \rho_i} \sum_{j=1}^N m_j \frac{\partial \phi_{ij}(h_i)}{\partial h_i}. \quad (12)$$

It should be noted that although the summations in Equations (8) to (12) are on all  $N$  particles, only the nearest neighbors contribute to the nonzero terms.

### 2.2. Plummer and Hernquist Model

Plummer (1911) introduced the Plummer model to fit the observed distribution of stars in globular clusters. It is basically a density model of a halo of matter, where the density function

is given by (Dehnen 2001)

$$\rho_P(r) = \frac{3GMr_s^2}{4\pi(r_s^2 + r^2)^{5/2}}, \quad (13)$$

where  $M$  is the total mass and  $r_s$  is a parameter that determines the concentration of the halo. The gravitation potential for this density function is given by

$$\phi_P(r) = -\frac{GM}{(r_s^2 + r^2)^{1/2}}. \quad (14)$$

Therefore the exact force acting on the  $i$ th particle of mass  $m$  at distance  $r$  will be given by

$$F_{\text{exact}}(r)_P = GMm \frac{r}{(r_s^2 + r^2)^{3/2}}. \quad (15)$$

Similarly, the density profile in the Hernquist model (Hernquist 1990) is calculated as

$$\rho_H(r) = \frac{GMr_s}{2\pi r(r_s + r)^3}. \quad (16)$$

The potential and exact force are given by (Hernquist 1990)

$$\phi_H(r) = -\frac{GM}{(r_s + r)}, \quad (17)$$

$$F_{\text{exact}}(r)_H = \frac{GMm}{(r_s + r)^2}. \quad (18)$$

### 2.3. Estimation of Errors

The exact force acting on each of the particles provided by any one of the models as described in Section 2.2 can be compared with the force calculated using Equations (2) and (10). Then, the average squared error (ASE) can be calculated as (Price & Monaghan 2007)

$$\text{ASE} = \frac{C}{N} \sum_{i=1}^N (F_{\text{exact}} - F_i)^2, \quad (19)$$

where  $C = 1/F_{\text{max}}^2$  is the normalization constant. Here  $F_{\text{max}}$  denotes the maximum value of the exact force. ASE strongly depends on the distribution of particles, and hence the error estimation from a system containing a relatively small number of particles does not provide a representative value of the true error. Such a dependency of the ASE on the distribution of particles in a system can be avoided by calculating the ASE values generated for many realizations obtained from the same model (Athanassoula et al. 2000). The average ASE value is then calculated from the results obtained by considering all such realizations. This average value of ASE, called the mass average square error (MASE), is defined as (Athanassoula et al. 2000)

$$\text{MASE} = \frac{C}{N} \left\langle \sum_{i=1}^N (F_{\text{exact}} - F_i)^2 \right\rangle. \quad (20)$$

### 2.4. The Problem of Pairing Instability

The problem of pairing instability arises during the SPH calculations due to the shape of the kernel gradient (Price 2012). The value of the kernel gradient tends towards

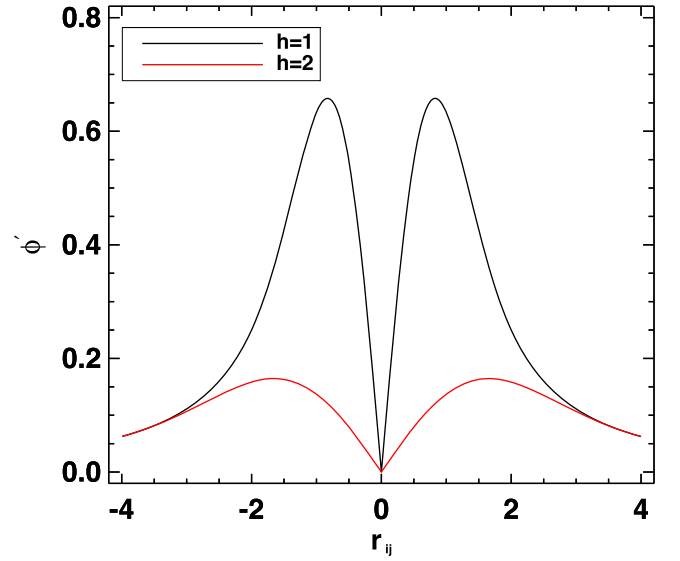


**Figure 1.** Kernel gradient ( $\phi'$ ) vs.  $r_{ij}$  for two different smoothing lengths  $\epsilon = 1.2$ .

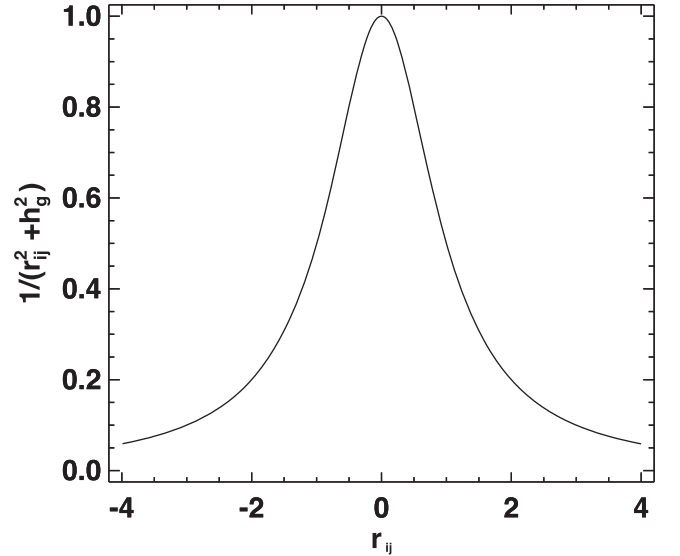


**Figure 2.** Plot of  $\left(\frac{1}{r_{ij}^2 + \epsilon^2}\right)$  vs.  $r_{ij}$  for smoothing length  $\epsilon = 1$ .

zero at the origin of the particle. As a result, when the particles approach very close to each other, their mutual gravitational force also becomes zero and forces these particles to create a separate group within the hump of the kernel gradient. The kernel gradient that is used in the gravitational force calculation is also not free from this problem, as shown in Figure 1. For example, if we increase the length of the smoothing length, the hump of the kernel gradient becomes approximately flat. Thus, it is extremely difficult to further increase the smoothing length for any calculations. This criterion automatically limits the value of  $\eta$  and hence one cannot choose the right optimal value of  $\eta$  according to the requirement of the calculation. This limitation puts a constraint on the accuracy of the calculation using the compact force method. On the other hand, in the noncompact force method, the pairing instability never arises. This can be ascertained from Figure 2. Thus one has the freedom to choose the right length of  $\epsilon_i$  to get minimum errors in the force calculation.

### 2.5. Adaptive Kernel Smoothing Length

In SPH,  $N_{\text{neigh}}$  is set a priori while determining the smoothing length of the particle that will interact with it. The latter varies accordingly to accommodate for the number of neighbors requested. Generally, there are two types of smoothing lengths; namely, fixed smoothing length and adaptive smoothing length. For systems where the density does not vary significantly with space and time, the fixed smoothing length is preferred as it requires less expensive calculations. However for systems with variable densities, which is a function of space and time, it is recommended to choose an individual (adaptive) smoothing length. The adoption of length helps to achieve a constant resolution at every point. In the adaptive method, the smoothing length ( $h_i$ ) varies as a function of the density given by (Price & Monaghan 2007)

$$h_i \propto \left(\frac{1}{\rho_i}\right)^{\frac{1}{3}} \Rightarrow h_i = \eta \left(\frac{m_i}{\rho_i}\right)^{\frac{1}{3}}. \quad (21)$$

The derivative of this is given by

$$\frac{\partial h_i}{\partial \rho_i} = -\frac{h_i}{3\rho_i}. \quad (22)$$

Springel & Hernquist (2002) used the following expression to preserve the constant resolution at every point,

$$N_{\text{neigh}} = \frac{4}{3}\pi(\sigma\eta)^3, \quad (23)$$

where  $\sigma$  is the compact support radius and is equal to 2 for the cubic spline kernel. The density calculated using Equation (21) as well as that calculated with  $\rho_i = \sum m_j W(|\mathbf{r}_i - \mathbf{r}_j|, h_i)$  should have the same value, i.e.,

$$f(h_i) = \sum_{j=1}^N m_j W(|\mathbf{r}_i - \mathbf{r}_j|, h_i) - m_i \left(\frac{\eta}{h_i}\right)^3 \quad (24)$$

must be zero. The individual smoothing length for each particle can be obtained using the Newton–Raphson method,

$$h_{i+1} = h_i - \frac{f(h_i)}{f'(h_i)}, \quad (25)$$

where

$$f'(h_i) = -\frac{3\rho_i\Omega_i}{h_i}. \quad (26)$$

The criterion of convergence of  $h_i$  is obtained using the following condition,

$$\frac{|h_{i+1} - h_i|}{h_i} < \sigma, \quad (27)$$

where  $\sigma$  can be chosen depending on the desired level of accuracy. The Newton–Raphson method has the highest rate of convergence because it approximates the root for a given  $\sigma$  in very few iterations. However convergence is highly dependent on the initial choice of the root. In some cases, the method fails to determine the root. In those cases where the convergence of the root cannot be obtained using the Newton–Raphson method even after 20 iterations, the root may be determined with the

help of the bisection method or other suitable root-finding methods.

### 2.6. Optimal Softening Length: A New Approach

Accuracy in gravitational force calculation depends on the choice of the optimal value of  $\epsilon$ . Price & Monaghan (2007) found that the individual optimal value of  $\epsilon_i \approx h_i$ . However, while calculating the appropriate optimal value of  $\epsilon_i$ , Equation (21), used in their study, has certain limitations. The equation contains a dimensionless parameter  $\eta$ , which is critical in determining  $N_{\text{neigh}}$ ; the choice of different values of  $\eta$  will lead to different error values in the calculation. Price & Monaghan (2007) also found that different values of  $N$  will have different corresponding  $\eta$  values for which the error is minimal. Due to the problem of pairing instability, Price & Monaghan (2007) adopted a fixed value of  $\eta = 1.2$ , which corresponds to  $N_{\text{neigh}} = 60$  in the Plummer density model. This value is not adequately appropriate for all possible configurations of the Plummer sphere. As the total number of particles ( $N$ ) is varied, the optimal value of  $\eta$  should also vary. Such a departure from the predetermined value of  $\eta$  may lead to a large error in the force calculation, which is undesirable. Furthermore, Zhu et al. (2015) showed that the numerical convergence in SPH calculations increases with the increasing value of  $N_{\text{neigh}}$  or  $\eta$ .

Therefore a suitable modification of the method, as prescribed by Price & Monaghan (2007), is needed while calculating the optimal value of  $\epsilon_i$  so that it is more adaptable in nature and can deal with different configurations of the Plummer model. In the present study we have been able to minimize this effect significantly in terms of accuracy and stability by introducing an additional variable termed as the “average characteristic length,” denoted by  $\lambda$  in the expression of  $\epsilon$ . With this modification, the expression of  $\epsilon$  becomes  $\epsilon_\lambda = \epsilon(\rho, \lambda)$ . We show that our new approach, as proposed in this study, can calculate the optimal value of  $\epsilon_{\lambda,i}$  for individual particles of a Plummer sphere more accurately as compared to the earlier studies. The results have been tested for both compact and noncompact forces.

#### 2.6.1. Average Characteristic Length

The optimal softening length of  $\epsilon$  depends on how particles are distributed as well as on  $N$ . Merritt (1996) found that the optimal softening length for  $N$  particles varies roughly as  $N^{-\frac{1}{3}}$ , which was later substantiated by Athanassoula (1998). The average spacing length also varies as  $N^{-\frac{1}{3}}$ . This implies that the optimal softening length should also vary linearly with the average spacing length of the system. In previous studies, a fixed value of  $\eta$  was used to characterize the average spacing length. But in the aforementioned discussion we have shown that as  $N$  varies, the average spacing length also varies linearly.

The optimal value of  $\epsilon$  for the whole system is a constant for a given configuration; but, in a localized scale inside the system, distribution of the particles varies from one place to the other. Therefore we calculate the ratio of the localized average spacing length for each particle to the average spacing length of the whole system. The value of this ratio varies from one particle to another. We call this ratio the “average characteristic length” and denote this dimensionless parameter as  $\lambda_i$ . In this study, we replace the constant term  $\eta$  with the variable term  $\lambda_i$  in order to calculate the more accurate optimal value of  $\epsilon_i$ . The

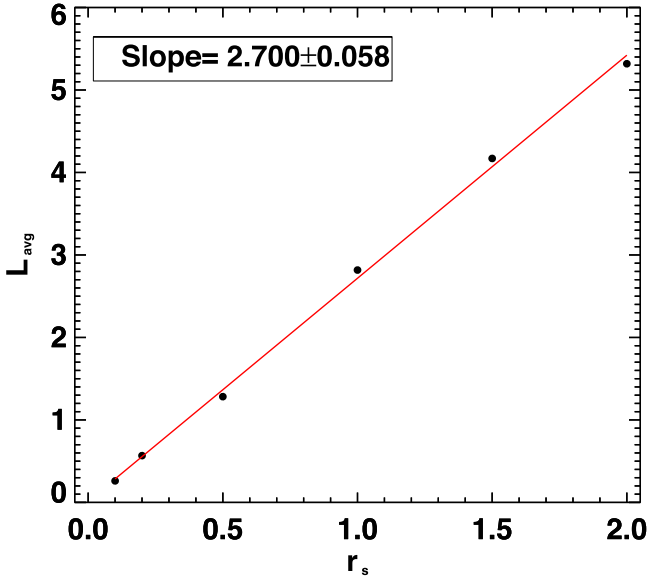


**Figure 3.** Plot of  $L_{\text{avg}}$  vs.  $r_s$  for the Plummer density model. The slope of the data points remains constant  $\approx 2.7$ , irrespective of the number of particles ( $N$ ) considered.

average spacing length of each particle is given by

$$l_{i,\text{avg}} = \frac{\sum_{j=1}^{N_{\text{neigh}}} r_{ij}}{N_{\text{neigh}} - 1}. \quad (28)$$

Now we introduce a new length called the average spacing length ( $L_{\text{avg}}$ ) of the system defined as

$$L_{\text{avg}} = \frac{1}{N} \sum_{i=1}^N l_{i,\text{avg}}. \quad (29)$$

This new parameter has been defined in order to observe the variations in the local distribution of  $N_{\text{neigh}}$  with respect to the total number of particles in the system. One of the intriguing properties of  $L_{\text{avg}}$  observed in this study is that the parameter is independent of  $N$  and depends only on  $r_s$  as given by  $L_{\text{avg}} \approx 2.7r_s$  for the Plummer density model as shown in Figure 3. For example, if  $r_s = 1$ , then  $L_{\text{avg}} \approx 2.7$  for the Plummer density model and similarly  $L_{\text{avg}} \approx 13.1$  for Hernquist density model, irrespective of any choice of  $N$  values.

Now considering the entire Plummer sphere, if  $L_{\text{avg}} = 2.7$ , then we set the corresponding value of  $r_s$  as equal to 1. Therefore for each  $i$ th particle in the Plummer density model with different  $l_{i,\text{avg}}$  values, the corresponding average characteristic length will be given by

$$\lambda_i = \frac{l_{i,\text{avg}}}{2.7} \text{ for } r_s = 1. \quad (30)$$

Further, we show that the optimal value of  $\epsilon_{\lambda,i}$  varies linearly with  $\lambda_i$ . In Figure 4 we have plotted the MASE versus  $\epsilon$  with  $r_s$  values 0.5, 1.0, and 2.0 for the Plummer density model considering  $N = 1000$ . It can be seen from the figure that the optimal softening length of  $\epsilon$  varies linearly with  $r_s$ . We have already shown that  $L_{\text{avg}} \propto r_s$  for the system. These imply that the optimal value of  $\epsilon$  varies linearly with  $L_{\text{avg}}$ . This suggests a linear dependence between the optimal value of  $\epsilon_i$  with  $\lambda_i$  in the localized scale.

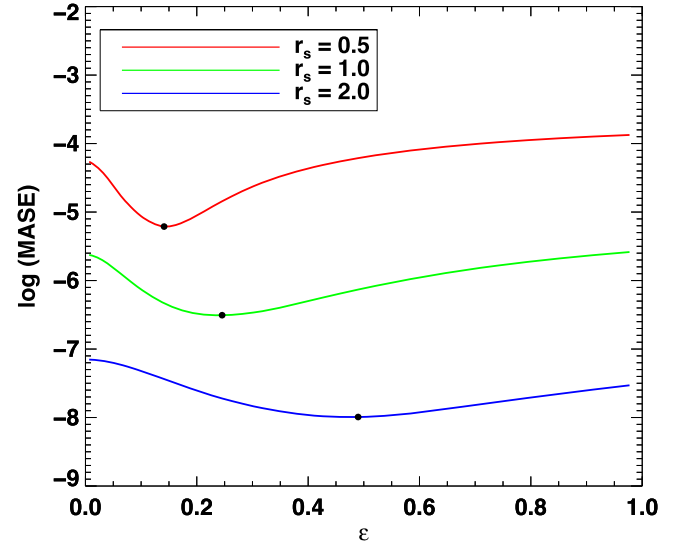


**Figure 4.**  $\log(\text{MASE})$  vs. softening length ( $\epsilon$ ) for the Plummer density model with  $N = 1000$ .

Therefore, based on the above justification,  $\epsilon_i$  is calculated by modifying Equation (21) as

$$\epsilon_{\lambda,i} = \lambda_i \left( \frac{m_i}{\rho_i} \right)^{\frac{1}{3}}. \quad (31)$$

The derivative of this is given by

$$\frac{\partial \epsilon_{\lambda,i}}{\partial \rho_i} = -\frac{\epsilon_{\lambda,i}}{3\rho_i}. \quad (32)$$

### 3. Results and Analysis

#### 3.1. Testing of Previous and New Equations

The value of the exact force at a given  $\mathbf{r}$  can be known from the Plummer (and also Hernquist) model(s). Using the previous methods, as described in Section (2), the force calculations for each of the particles can be carried out based on Equation (21). This equation relies on  $\eta$ , which has to be fixed before the force calculation is done.

In order to test the methods described in the previous section, we generate various values of  $\epsilon_i$  from  $10^{-3}$  to  $10^{0.5}$  for each of the particles in the Plummer model using a step size of 0.003, which is added to the power of the previous incremental value. Using each  $\epsilon_i$  value thus generated, the error in the force calculation is obtained for individual particles. The optimal value of  $\epsilon_i$  for a particle is chosen that gives the minimum value of the error in the force calculation. All such optimal values of  $\epsilon_i$  obtained for each of the particles are considered as data for a given number of particles in the system. The data are then fitted with the earlier methods and our new methods.

We now present a comparative analysis of the data for accurately evaluating the optimal value of  $\epsilon_i$  in the Plummer sphere with different configurations of its constituent particles. The noncompact force is calculated as given in Equation (2) to calculate the exact optimal value of  $\epsilon_i$  for two Plummer spheres with  $N = 100$  and  $N = 1000$  particles using two fixed  $\eta$  values for each configuration. The analysis is performed using  $M = 1$  and  $r_s = 1$  in all cases. Figure 5 shows a plot of normalized  $\rho_i$  versus optimal  $\epsilon_i$  for the configuration  $N = 100$  using two fixed  $\eta$  values 0.8 and 1.2, respectively. Similarly, Figure 6 depicts



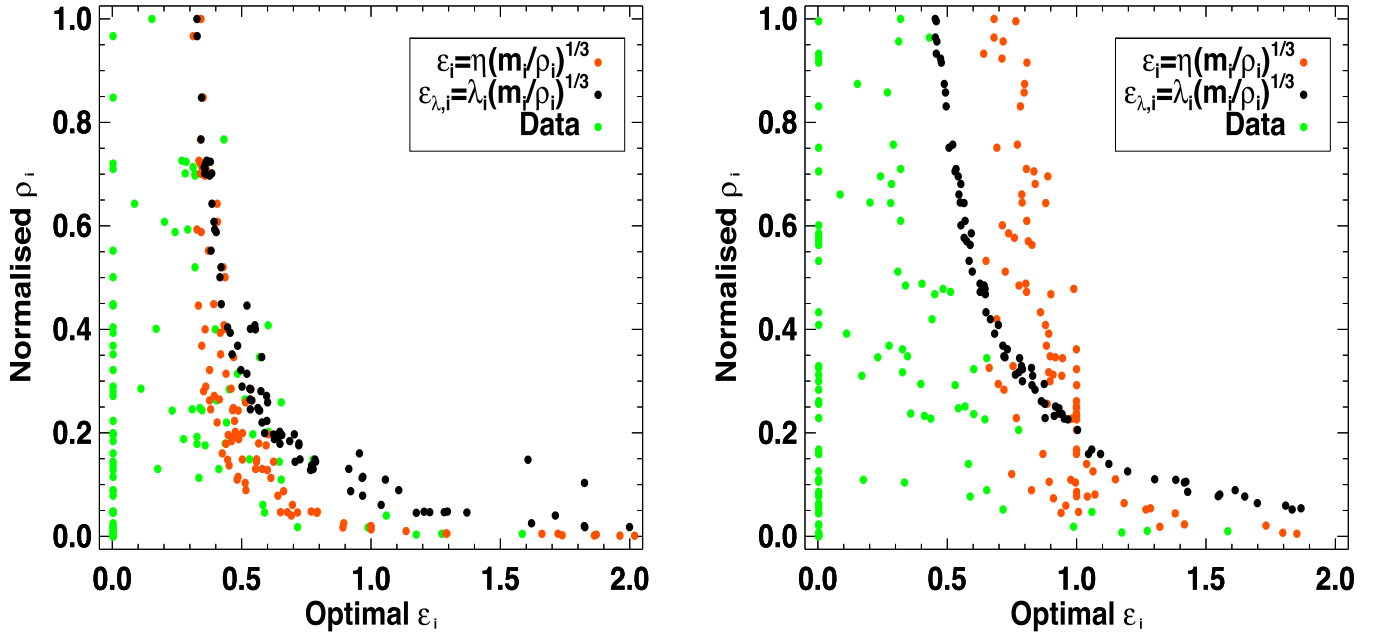


**Figure 5.** Left panel:  $\rho_i$  vs. optimal  $\epsilon_i$  for  $\eta = 0.8$  and  $N = 100$ . Right panel:  $\rho_i$  vs. optimal  $\epsilon_i$  for  $\eta = 1.2$  and  $N = 100$ . Force calculations in both the panels are carried out using a noncompact force. The green-colored points indicate the numerically generated data as described in the text. Red- and black-colored points denote optimal  $\epsilon_i$  values obtained from the earlier and the present study, respectively.

the same for the configuration  $N = 1000$  using two fixed  $\eta$  values 1.2 and 2.5, respectively. It is to be noted that Equation (2) is valid only when  $\epsilon$  is constant. Since each particle has a different softening length in the adaptive method that we have formulated, Equation (2) in its present form cannot be used. In order to make this valid for varying the softening length,  $\epsilon$  is replaced with  $\epsilon_i$  for the results presented in Figures 5 and 6. While doing this the symmetric form of Equation (2) will be lost. Therefore the equation is symmetrized using Equation (6) by considering  $\phi'$  of the form given by Equation (7). This treatment on Equation (2) has been used in further calculation of this study. These figures show that the  $\eta = 1.2$  condition is valid only for a specific value of  $N$  and is unable to trace the data for other configurations of the Plummer sphere. In other words, different choices of  $N$  in the Plummer sphere result in different values of  $\eta$ , which provides a better tracing in the force calculation. For example, if  $N = 100$ , then  $\eta = 1.2$  is not the best choice and instead  $\eta = 0.8$  provides a much improved representation, as shown in Figure 5. However with  $N = 1000$ , the  $\eta = 1.2$  imposition in Equation (21) provides an excellent matching, while  $\eta = 2.5$  results in an undesirable fitting for the same particle density in the Plummer sphere, as shown in Figure 6.

We carry out a similar analysis using compact force calculations with  $N = 1000$  for fixed  $\eta = 1.2$ . Since we do not know the exact relation between  $h_i$ , i.e.,  $\epsilon_i$  and  $\rho_i$ , beforehand, the second term of Equation (6) is not used for the calculation of force for Figure 7 initially, as it requires the calculation of the derivative of  $\epsilon$ . An initial guess of the optimal value of  $\epsilon_i$  can be determined because the second term is small compared to the first term (Price & Monaghan 2007). Figure 7 shows the plot of normalized  $\rho_i$  versus optimal  $\epsilon_i$  for the configuration  $N = 1000$  using fixed  $\eta = 1.2$ . This figure again shows that  $\eta = 1.2$  is not the best choice for this configuration.

### 3.2. Force Calculation Using Our Modified Equation

In order to overcome the critical problem in force calculations as discussed in the previous section, we use our modified Equation (31). The results obtained from our analysis show that the data for various configurations (corresponding to different values of  $\eta$  and  $N$ ) can be fitted reliably by using this equation. The black-colored points in Figures 5–7 illustrate how the modified form of  $\epsilon_{\lambda,i}$ , as formulated in this study, fits the data more accurately than the original form of  $\epsilon_i$  with  $\eta = 1.2$ , i.e., for  $N_{\text{neigh}} = 60$ .

### 3.3. Imposing a New Condition

We find that the gravitational force calculated using Equation (2) produces as much as 30–40% of the total number of particles satisfying the condition  $\epsilon_i \approx 0$ , thereby generating nonzero values of  $\epsilon_i$  for the remaining particles, as illustrated in Figures 5 and 6. This results in higher values of the MASE in noncompact force, as Equation (21) fails to trace particles with the condition  $\epsilon_i \approx 0$ . Thus,  $\epsilon_i$  does not simply vary as a function of density as observed from these plots. Also the particles with  $\epsilon_i \approx 0$  are difficult to distinguish from the remaining particles in the  $\epsilon_i$ – $\rho_i$  plane. Furthermore, we find that the calculation of gravitational force using Equation (10) leads to about 10% of total particles with an optimal value of  $\epsilon_i \approx 0$ , whereas the remaining particles have nonzero values of  $\epsilon_i$ , as can be seen in Figure 7.

As the number of particles satisfying the condition of the optimal value of  $\epsilon_i \approx 0$  are quite large in number for compact as well as noncompact forces, it is very difficult to classify the remaining particles ( $\epsilon_i \neq 0$ ) on the basis of  $\rho_i$ . We found that such particles with nonzero values of  $\epsilon_i$  roughly obey the following relation:

$$F_{\text{exact},i} > \sum_{j=1}^N \frac{Gm_i m_j}{r_{ij}^2}. \quad (33)$$

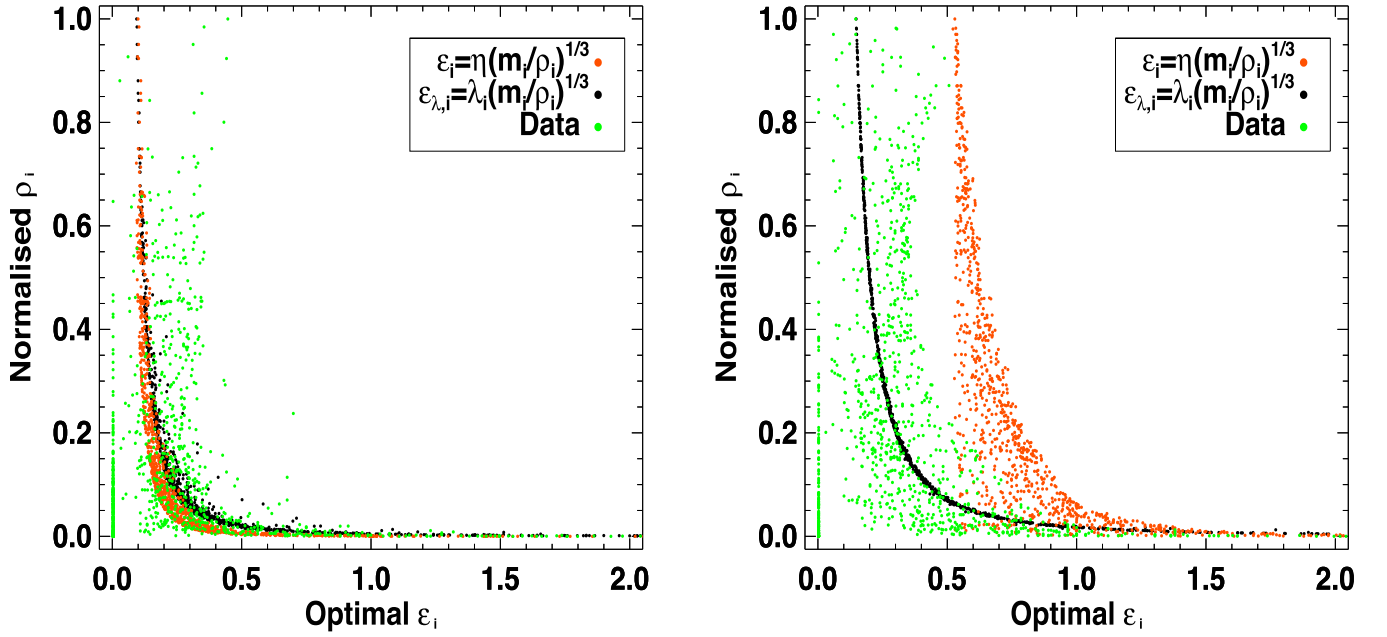


**Figure 6.** Left panel:  $\rho_i$  vs. optimal  $\epsilon_i$  for  $\eta = 1.2$  and  $N = 1000$ . Right panel:  $\rho_i$  vs. optimal  $\epsilon_i$  for  $\eta = 2.5$  and  $N = 1000$ . Force calculations in both the panels are carried out using noncompact force. The green-colored points indicate the numerically generated data as described in the text. Red- and black-colored points denote optimal  $\epsilon_i$  values obtained from the earlier and the present study, respectively.

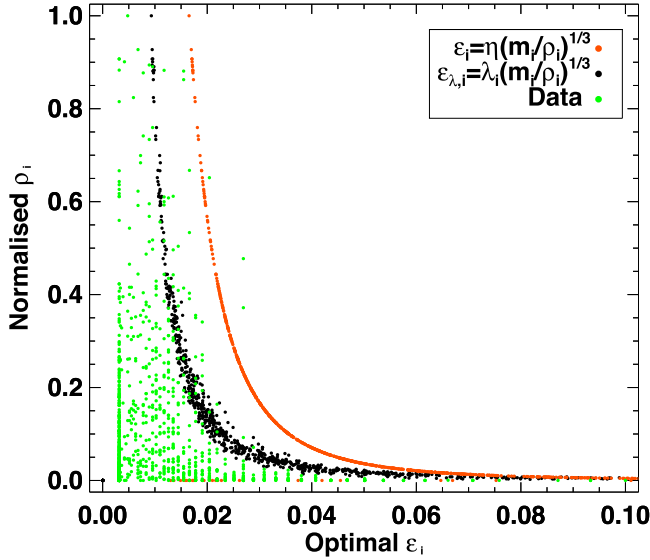


**Figure 7.** Plot of optimal  $\epsilon_i$  vs. normalized  $\rho_i$  with  $r_s = 1$ ,  $M = 1$ ,  $\eta = 1.2$ , and  $N = 1000$  for the Plummer density model using compact force. Red- and black-colored points denote optimal  $\epsilon_i$  values obtained from the earlier and the present study, respectively.

This is depicted in Figure 8. We also incorporate the following conditional statement while calculating ASE,

$$\begin{aligned}
 &\text{Initialize ASE} = 0 \\
 &\text{for } i = 1 \text{ to } N: \\
 &\quad \text{if } |F_{\text{exact},i} - F_i|_{\epsilon_i=0} < |F_{\text{exact},i} - F_i|_{\epsilon_i=\epsilon_{\lambda,i}}: \\
 &\quad \quad \text{ASE} = \text{ASE} + \frac{C}{N} (F_{\text{exact},i} - F_i)_{\epsilon_i=0}^2 \\
 &\quad \text{else: ASE} = \text{ASE} + \frac{C}{N} (F_{\text{exact},i} - F_i)_{\epsilon_i=\epsilon_{\lambda,i}}^2 \\
 &\text{endfor.}
 \end{aligned} \tag{34}$$

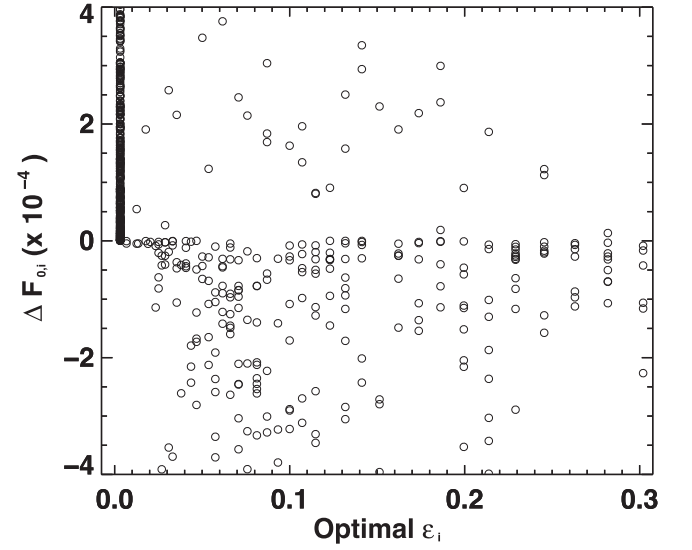


**Figure 8.**  $\Delta F_{0,i}$  vs. optimal  $\epsilon_i$  with  $r_s = 1$ ,  $M = 1$ , and  $N = 1000$  for the Plummer density model where  $\Delta F_{0,i} = F_{\text{exact},i} - \sum_{j=1}^N \frac{Gm_i m_j r_{ij}}{(r_{ij}^2 + \epsilon_i^2)^{3/2}}$ .

Here  $F_i$  can be a compact or a noncompact force. Imposition of the conditions given by Equation (34) decreases the error in the force calculation as well as making the  $\epsilon$  versus the MASE plot significantly flat for higher values of  $\epsilon$  as depicted in Figure 9. The flat nature of the MASE obtained for higher values of  $\epsilon$  has a larger implication as the error in the force calculation does not increase appreciably for values of  $\epsilon$  far from the optimal value.

We have found that the MASE values remain almost flat for a wide consideration of  $N_{\text{neigh}}$  and it closely follows the corresponding minimum MASE values predicted by previous studies for a particular  $N_{\text{neigh}}$ , as shown in Figure 10. Based on

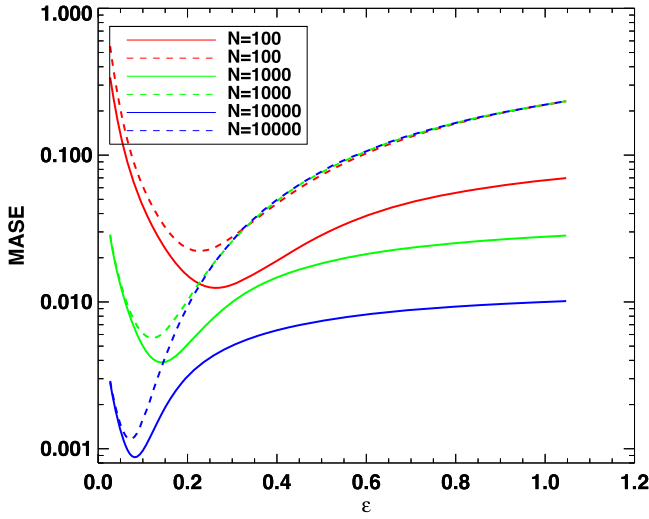


**Figure 9.** MASE vs. fixed  $\epsilon$  for different numbers of particles for  $r_s = 1$  and  $M = 1$  using noncompact force. Solid lines represent MASE values calculated using Equations (2) and (34), whereas the dashed lines depict the plots of the MASE calculated using Equation (2), only without the condition given by Equation (34).

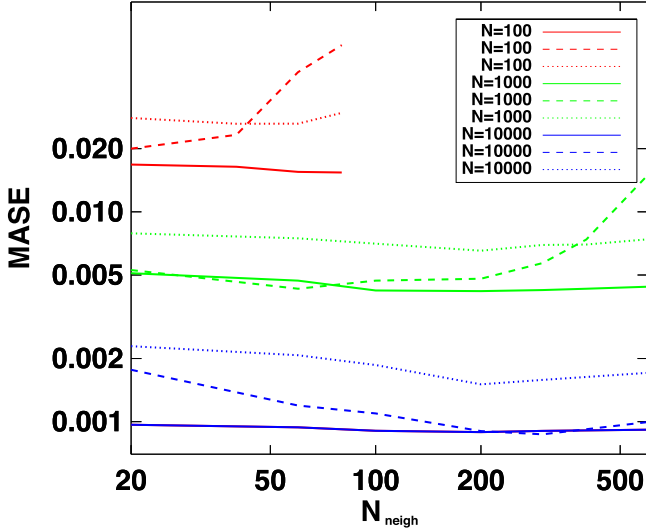


**Figure 10.**  $N_{\text{neigh}}$  vs. MASE with  $r_s = 1$  and  $M = 1$  for different numbers of particles in the Plummer density model. The MASE is calculated using Equation (20). The solid line represents the MASE values calculated with the help of Equation (31) where we have used the symmetric form of Equation (2) (noncompact force) along with the condition given by Equation (34). The dashed line is obtained using Equation (10) (compact force) and Equation (21). The dotted line represents the MASE values obtained using Equation (10) and Equation (31) for compact force.

these findings we conclude that our equation given by Equation (31) is more adaptive and appropriate for resolving better accuracy in force calculations for different configurations of particles in a Plummer sphere. Thus the consideration of a universal value of  $\eta$  (i.e., 1.2) in Equation (21) cannot always provide the correct optimal value of  $\epsilon_i$ . Due to the problem of pairing instability in SPH,  $\eta$  cannot be treated as a free parameter. Hence Price (2012) fixed  $\eta$  as 1.2 for all configurations of the Plummer sphere in their study. However, this criterion turns out to be a limiting factor for achieving minimum error in the gravitational force calculation for different Plummer configurations. The effect of such limitation for a fixed  $\eta$  value is illustrated in Figure 10 where we have

determined the MASE values for different considerations of  $N$ . It is found that the optimal  $\eta$  value (Equation (21)) for which the MASE will be a minimum is different corresponding to different values of  $N$ . Therefore with  $\eta = 1.2$ , the minimum error is not achievable for all configurations of the Plummer sphere.

#### 4. Summary and Conclusion

This study offers a novel approach in significantly enhancing the accuracy of gravitational force calculations dealing with the  $N$ -body simulations for the Plummer density model as compared to the earlier studies. The optimal softening length ( $\epsilon_i$ ) is an important parameter while calculating gravitational forces in  $N$ -body simulations. Since the accuracy in the force calculations is strongly dependent on the choice of  $\epsilon_i$ , there is a need to critically evaluate this crucial parameter. This study takes into account various aspects that can influence the calculations while determining the optimal value of  $\epsilon_i$  and thereby minimizing the error in the force calculations. The results obtained from this study are enumerated as follows:

- (i) We find that the gravitational force calculation produces a large fraction of particles with optimal values of  $\epsilon_i \approx 0$ . We show that the number of such particles can be more than 30% and 10% of the total number of particles in the Plummer sphere for noncompact (Equation (2)) and compact force (Equation (10)) calculations, respectively. As such a fraction of particles with  $\epsilon_i \approx 0$  is statistically large, we impose an additional condition while calculating the optimal value of  $\epsilon_{\lambda,i}$ . Our method of force calculation significantly improves the accuracy and remarkably decreases the error in the gravitational force calculations. Furthermore, this technique has a larger implication in the error calculations because of the flat nature of the MASE obtained for higher values of  $\epsilon_{\lambda,i}$ .
- (ii) A major drawback of the existing techniques for calculating the optimal value of  $\epsilon_i$  is that they depend to a large extent on  $N_{\text{neigh}}$ . This problem has been overcome in the present study by introducing a new technique to calculate the optimal value of  $\epsilon_{\lambda,i}$ , which is assumed to be a function of  $\rho_i$  and  $\lambda_i$ . In SPH, the smoothing length  $h_i$  depends on  $\eta$ . The density at a point is determined based on the value of  $h_i$  incorporated into the kernel function. Variation of  $h_i$  (or  $\eta$ ) produces a very small variation in the  $\rho_i$  value. This ensures that this new method has less dependency over  $\eta$  as compared to the earlier method and also overcomes the problem of pairing instability. Thus the accuracy in the force calculation is quite independent of  $\eta$ . This implies that the new modified Equation (31) is more adaptive in nature and hence can be used for any configurations of the Plummer density model.

A.B. acknowledges the financial support of this study provided by the Department of Science and Technology, Science and Engineering Research Board (DST-SERB), Govt. of India, New Delhi, through the research grant “ECR/2016/002045.” S.D. thanks Council of Scientific and Industrial Research (CSIR), Govt. of India, New Delhi, for financial support through the research grant “03(1425)/18/EMR-II.” The authors thank the anonymous referee for providing a set of constructive comments and valuable suggestions, which significantly helped in improving the manuscript.



## ORCID iDs

Amiya Baruah  <https://orcid.org/0000-0001-7951-4896>

## References

- Asphaug, E., Agnor, C. B., & Williams, Q. 2006, *Natur*, **439**, 155
- Athanassoula, E. 1998, *NYASA*, **867**, 141
- Athanassoula, E., Fady, E., Lambert, J. C., & Bosma, A. 2000, *MNRAS*, **314**, 475
- Balsara, D. S. 1995, *JCoPh*, **121**, 357
- Barnes, J., & Hut, P. 1986, *Natur*, **324**, 446
- Bate, M. R., & Burkert, A. 1997, *MNRAS*, **288**, 1060
- Bui, H. H., & Nguyen, G. D. 2017, *IJSS*, **125**, 244
- Couchman, H. M. P., Thomas, P. A., & Pearce, F. R. 1995, *ApJ*, **452**, 797
- Davé, R., Dubinski, J., & Hernquist, L. 1997, *NewA*, **2**, 277
- Davis, B. L., Graham, A. W., & Cameron, E. 2019, *ApJ*, **873**, 85
- Dehnen, W. 2001, *MNRAS*, **324**, 273
- Dyer, C. C., & Ip, P. S. S. 1993, *ApJ*, **409**, 60
- Federrath, C., Banerjee, R., Clark, P. C., & Klessen, R. S. 2010, *ApJ*, **713**, 269
- Flebbe, O., Muenzel, S., Herold, H., Riffert, H., & Ruder, H. 1994, *ApJ*, **431**, 754
- Gingold, R. A., & Monaghan, J. J. 1977, *MNRAS*, **181**, 375
- Hernquist, L. 1990, *ApJ*, **356**, 359
- Hosono, N., Saitoh, T. R., & Makino, J. 2013, *PASJ*, **65**, 108
- Hosono, N., Saitoh, T. R., Makino, J., Genda, H., & Ida, S. 2016, *Icar*, **271**, 131
- Katz, N., Weinberg, D. H., & Hernquist, L. 1996, *ApJS*, **105**, 19
- Lia, C., & Carraro, G. 2000, *MNRAS*, **314**, 145
- Lucy, L. B. 1977, *AJ*, **82**, 1013
- Malamud, U., & Perets, H. B. 2020, *MNRAS*, **492**, 5561
- Merlin, E., Buonomo, U., Grassi, T., Piován, L., & Chiosi, C. 2010, *A&A*, **513**, A36
- Merritt, D. 1996, *AJ*, **111**, 2462
- Owen, J. M., Villumsen, J. V., Shapiro, P. R., & Martel, H. 1998, *ApJS*, **116**, 155
- Petschek, A., & Libersky, L. 1993, *JCoPh*, **109**, 76
- Plummer, H. C. 1911, *MNRAS*, **71**, 460
- Price, D. J. 2008, *JCoPh*, **227**, 10040
- Price, D. J. 2012, *JCoPh*, **231**, 759
- Price, D. J., & Monaghan, J. J. 2007, *MNRAS*, **374**, 1347
- Price, D. J., Wurster, J., Tricco, T. S., et al. 2018, *PASA*, **35**, e031
- Quinlan, N., Basa, M., & MM, L. 2006, *IJNME*, **66**, 2064
- Rasio, F. A., & Livio, M. 1996, *ApJ*, **471**, 366
- Rodionov, S. A., & Sotnikova, N. Y. 2005, *ARep*, **49**, 470
- Romeo Velonà, A. D., Sommer-Larsen, J., Napolitano, N. R., et al. 2013, *ApJ*, **770**, 155
- Schäfer, C., Riecker, S., Maindl, T. I., et al. 2016, *A&A*, **590**, A19
- Springel, V., & Hernquist, L. 2002, *MNRAS*, **333**, 649
- Sun, P.-N., Le Touzé, D., Oger, G., & Zhang, A.-M. 2021, *JCoPh*, **426**, 109936
- Tartakovsky, A., & Meakin, P. 2005, *PhRvE*, **72**, 026301
- Valcke, S., de Rijcke, S., Rödiger, E., & Dejonghe, H. 2010, *MNRAS*, **408**, 71
- Wadsley, J. W., Stadel, J., & Quinn, T. 2004, *NewA*, **9**, 137
- Zhu, Q., Hernquist, L., & Li, Y. 2015, *ApJ*, **800**, 6